GLOBAL BIOGEOCHEMICAL CYCLES, VOL. 10, NO. 2, PAGES 347–359, JUNE 1996

Sources and sinks of carbon monoxide in the mixed layer of the tropical South Pacific Ocean

James E. Johnson[2,1] and Timothy S. Bates[1,2]

Abstract. The magnitude of the oceanic source of carbon monoxide (CO) to the atmosphere depends on the concentration of CO in ocean surface waters. To ascertain the relative importance of the processes controlling this concentration, depth profiles of CO concentrations in the oceanic mixed layer and upper thermocline were made at two time series stations in the tropical Pacific Ocean during 1993. The two stations were chosen to contrast an oligotrophic region of low CO water concentrations (RITS93) with a biologically productive region of high seawater CO concentrations (RITS94). The column burden of CO in the upper 75 m of the water column averaged 53 μmole m^{-2} at the RITS93 station and 240 μmole m^{-2} at the RITS94 station. From the observed diurnal cycle of the CO column burden, production and loss rates at each site were estimated. The factor of 4.5 difference in the column burden is primarily due to a smaller in situ oxidation rate constant at the RITS94 site.

Introduction

Carbon monoxide is one of the most important reactive gases in the atmosphere because its reaction with the hydroxyl radical, OH, is the major sink of atmospheric OH [*Thompson and Cicerone*, 1986]. Although the dominant sources of atmospheric CO are continental and anthropogenic [*Müller*, 1992], the surface waters of the world's oceans are supersaturated with CO with respect to the atmosphere and thus the ocean is also a source of atmospheric CO [*Swinnerton et al.*, 1970; *Seiler and Schmidt*, 1974; *Conrad et al.*, 1982]. This sea-to-air flux varies seasonally and regionally from 0.25 to 13 μmole m^{-2} d^{-1} [*Bates et al.*, 1995] and is determined primarily by the oceanic CO concentration. The processes controlling this oceanic CO concentration must be understood in order to predict how CO emissions might change with a changing climate.

The major source of CO in the surface waters of the ocean is the abiotic photo-oxidation of dissolved organic carbon (DOC) initiated by UV light [*Redden*, 1983; *Mopper et al.*, 1991; *Valentine and Zepp*, 1993]. The major sinks are microbial oxidation and flux to the atmosphere [*Conrad and Seiler*, 1980, 1982; *Jones*, 1991]. The lifetime of CO in the water column has been shown to range from hours to days [*Jones*, 1991]. Because of this short lifetime, CO exhibits high variability in both time and space.

Because of the diurnal nature of its photochemical production, large diurnal cycles of CO in surface water are expected and have been observed since measurements began in the 1960s [*Swinnerton and Lamontagne*, 1974; *Conrad et al.*, 1982]. These diurnal cycles generally show increasing concentrations of CO from morning to a maximum in middle to late afternoon, followed by a rapid decline in the early evening. The relative magnitude of these cycles varies and can result in diurnal changes in concentration by as much as a factor of 2 [*Conrad et al.*, 1982].

Surface water CO concentrations have been shown to vary regionally and seasonally. There is a strong gradient [*Swinnerton and Lamontagne*, 1974; *Bates et al.*, 1995] between the low CO concentrations found in tropical oligotrophic water poleward of 5° (<1 nM) and the high concentrations found in the biologically productive equatorial waters (2–6 nM). This gradient exists even though both regions experience very similar solar UV fluxes and thus potentially similar photochemical sources. In temperate and high latitudes, a large seasonal cycle in daily mean CO concentrations has been observed [*Bates et al.*, 1995] which is explained by the seasonal nature of the photochemical source.

Although the variability of CO concentrations in oceanic surface water can in theory be predicted from the rate constants of the source and sinks, in practice these rate constants and the factors controlling them are not well known. Field observations have the potential to reduce the uncertainty associated with these rate constants. Because the photochemical source requires UV light, and because UV light is rapidly attenuated with depth, the strongest gradients of dissolved CO occur in the vertical, with maximum concentrations at or near the surface. Although these profiles have been measured on a few occasions [*Conrad et al.*, 1982; *Jones*, 1991], there have been no reports of detailed time series of CO concentration measurements in the oceanic mixed layer. This study describes time series of CO concentration profiles in the mixed layer and the upper thermocline at two distinctly different locations in the tropical Pacific Ocean. From the observed changes in the CO vertical profiles at each station we estimate loss and production rates and we also propose a simple mathematical model that explains many features of the CO diurnal cycle.

[1]Pacific Marine Environmental Laboratory, NOAA, Seattle, Washington.

[2]Joint Institute for the Study of the Atmosphere and Ocean, University of Washington, Seattle.

Paper number 96GB00366
0886-6236/96/ 96GB-00366$12.00

Methods

Samples were collected in 10-L standard Niskin bottles fitted with silicone O-rings and Teflon-coated springs. Seawater samples were drawn from the Niskin bottles into 100-mL ground glass syringes without contact with the atmosphere. The syringes were stored in the dark in a bath of ambient seawater from the ship's clean sampling system which was within 1 degree of ambient surface seawater temperature. All samples were analyzed within 3 hours of collection.

Seawater from each syringe was transferred into a 37-mL glass loop connected to a 10-port Valco GC sampling valve. At least 80 mL of seawater were transferred out of each syringe to purge and fill the loop. The Valco valve was then switched and 40 mL/min of He (the stripper flow) pushed the seawater sample out of the glass loop and into a glass stripping vessel fitted with a bottom frit. Once the sample was transferred, the He flow continued for an additional 3 min to purge the sample of dissolved gases. The He effluent from the stripping vessel was directed first through an empty stainless steel loop held at –35°C to trap water vapor, then through a second stainless steel loop (preconcentrator) packed with 60/80 mesh molecular sieve 5A, also held at –35°C. Both of these loops were attached to a second 10-port Valco GC sample valve. After the stripping/collection period the second Valco valve was switched, directing 40 mL/min of a carrier gas stream of He through the preconcentrator (but not the water trap), and the preconcentrator was rapidly heated to 180°C. This heating injected the trapped gasses into the carrier gas, which then flowed through a molecular sieve 5A separation column and into a hot mercuric oxide reduction detector (RGD2, Trace Analytical Inc., Menlo Park, Calif.). The only modification of the detector was the replacement of its internal temperature controller and sensor with a Pt RTD sensor and an external temperature controller (CN911A, Omega, Stamford, Conn.). This greatly improved the detector stability. The output of the detector was digitized, integrated, and stored on a computer that also controlled all of the valve switching and preconcentrator heating and cooling. The only manual operation was the initial transfer of the seawater sample out of the syringe. Each sample required 12 min of analysis time, so approximately 5 samples could be analyzed per hour.

The analysis system was standardized by injecting known volumes of standard gas, at a known temperature and pressure, through the entire analysis system. The gas standards were calibrated against standards at the National Oceanic and Atmospheric Administration/Climate Monitoring and Diagnostics Laboratory (NOAA/CMDL). The CMDL standard is fully described by *Novelli et al.* [1991]. Further details of the PMEL CO standards are described by *Bates et al.* [1995]. The stability of the detector to the standards was such that over a typical 5-day period on the RITS94 cruise, a standard, comparable in CO content to the surface water samples, was injected a total of 98 times, yielding a sigma/mean in the detector response of 2.7%.

At each station the sampling, storage, and analysis system was evaluated by closing all (11 on RITS93, 12 on RITS94) Niskin bottles at 750 m depth. These samples were analyzed for CO with a resulting concentration of 0.21 ± 0.053 nM on RITS93 and 0.20 ± 0.04 nM on RITS94 (mean ± standard deviation). This measured CO may be a sample blank from contamination from the Niskin bottles or from the sample syringes. It also may represent a background concentration maintained by nonphotochemical sources, as it is roughly equivalent to previously reported CO concentrations below the photic zone [*Conrad et al.*, 1982; *Jones*, 1991]. Because the surface concentrations of CO were much lower at the RITS93 time series station, this deep concentration was a larger percentage of the mean surface concentration during RITS93 (20%) than during RITS94 (5.6%).

Seven times during the RITS93 time series station, duplicate samples were collected from the same Niskin bottle. The average concentration in these seven pairs was 0.78 nM, and within each pair the average difference was 0.077 nM, or 9.4%. At both time series stations we have conservatively assumed that at concentrations less than 0.78 nM the sampling error was ±0.039 nM and at concentrations greater than 0.78 nM the sampling error was ±4.7%.

At both stations, depth profiles of temperature and salinity were measured with the ship's conductivity-temperature-depth (CTD) system (Seabird). Time series of total solar radiation (insolation) were measured at each station with the same Epply radiometer. One profile of UV light penetration was measured at the RITS93 station with an underwater radiometer (Biospherical Instrument, Inc., model PUV 500) that measured irradiance at four wavelengths (308, 320, 340, and 380 nm) and returned data at 1-m intervals. One profile of UV light penetration at the RITS94 station was measured with an underwater spectroradiometer (LI-COR Inc., LI-1800UW) which did complete scans at 5-m-depth intervals. In order to compare the two profiles, the irradiance at the four wavelengths measured in RITS93 were extracted from the RITS94 spectra.

The time series measurements were made aboard the NOAA ship *Surveyor*. The RITS93 time series station occurred during April 12–15, 1993, at 19°S, 149.5°W, approximately 100 km south of Tahiti, in oligotrophic waters characterized by very low nitrate (<0.05 μM) and chlorophyll (0.05 μg/L) levels in the mixed layer. The RITS93 station was Eulerian in that the ship stayed within 18 km of the station location. At this station, five CTD casts were made each day at 4-hour intervals, starting at 0530 local time (LT) each morning. After the first two casts, sample depths were standardized at 5, 10, 15, 20, 30, 40, 50, 75, 100, and 200 m.

The RITS94 time series station was occupied during December 6–10, 1993, and began at 4°00′S, 140°00′W. At this station, six CTD casts were made each day at 4-hour intervals, starting at 0230 LT each morning. Each cast included samples collected at 5, 10, 20, 30, 40, 50, 75, 100, 125, 150, 200, and 250 m. The RITS94 station was Lagrangian in that the ship remained with the same water mass by following a free drifting drogue. The measurements ended 4 days later at 4°34′S, 140°55′W. In contrast to the RITS93 station, the RITS94 station was located in nutrient-rich, biologically productive waters that had recently upwelled near the equator. During the RITS94 station the mean surface water nitrate concentration was 3.6 μM and the mean surface water chlorophyll concentration was 0.19 μg/L.

Results

Typical profiles of UV light penetration, temperature, and chlorophyll and CO concentrations for both time series are shown in Figure 1. For each station and wavelength, the 1% light level was found by fitting the measured irradiance to a straight line on a semilog plot. At the RITS93 station these 1% light

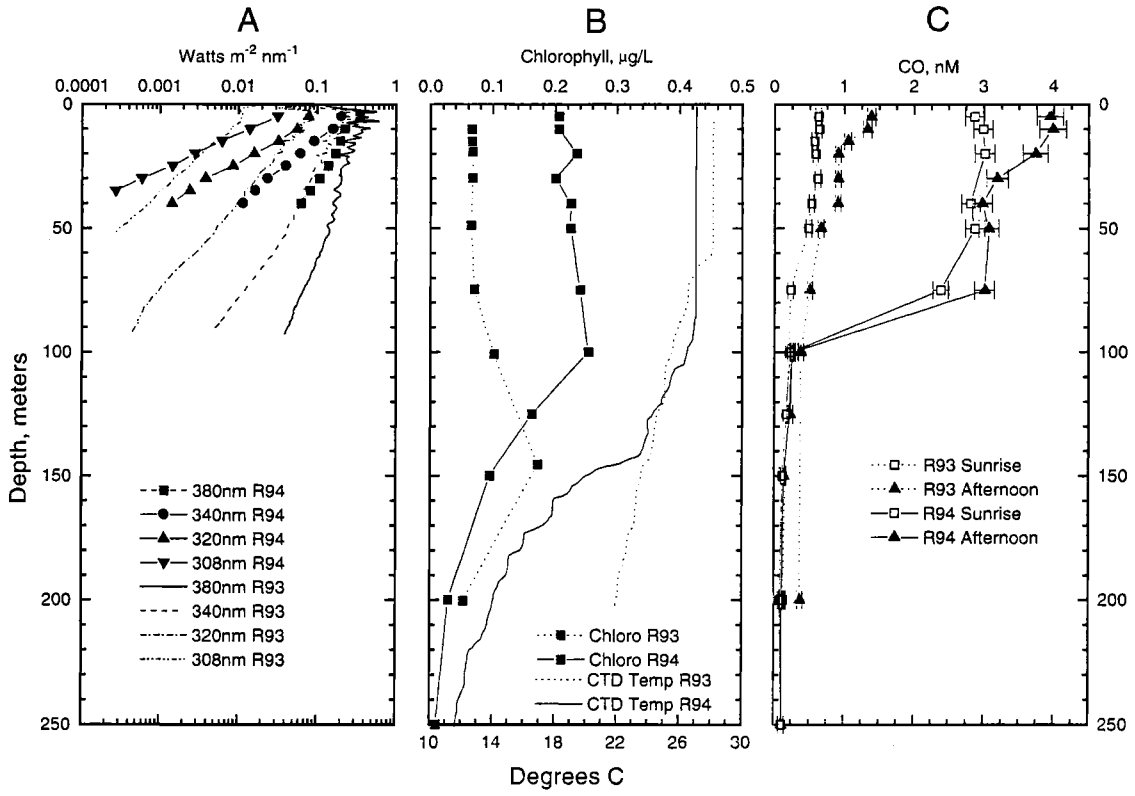

Figure 1. a) Light penetration at the indicated wavelengths in the mixed layer from RITS93 at 1400 local time (LT) on Day of Year (DOY) 103 and from RITS94 at 1200 LT on DOY 341. b) Chlorophyll and temperature profiles from RITS93 at 1130 LT on DOY 102 and from RITS94 at 1100 LT on DOY 340. c) CO profiles from RITS93 at 0530 and 1330 LT on DOY 103, and from RITS94 at 0630 and 1430 on DOY 341. The estimated sampling error is shown for each CO measurement as the greater of ±0.039 nM or ±4.7%.

levels were 60, 75, and 97 m at 308, 320, and 340 nm, respectively. The 380-nm 1% light level could not be calculated because at the bottom of the 90-m light cast the irradiance was still 12% of the surface value. The UV light profile shows that the seawater at the RITS93 time series station was among the clearest of natural seawaters [*Smith and Baker*, 1981; *Baker and Smith*, 1982]. In contrast, the seawater at the RITS94 station was less transparent and more typical of biologically rich seawater, with 1% light levels of 29, 38, 54, and 102 m at 308, 320, 340, and 340 nm, respectively.

The chlorophyll profiles (Figure 1b) at the RITS93 and RITS94 stations are clearly different, with mixed layer chlorophyll concentrations approximately 4 times greater at the RITS94 station. The temperatures from a typical cast at each station (Figure 1b) show that the mixed layer was twice as deep at the RITS94 station (100 versus 50 m) but the temperature gradient in the upper thermocline was weaker at the RITS93 station. Typical CO profiles from morning and late afternoon casts at each station are shown in Figure 1c. The daily production of CO is clearly apparent in each profile.

At the RITS93 station (Figure 2) the mixed layer depth varied from 45 to 85 m during the 3-day time series. The CO concentrations decreased with depth, with no clear break at the bottom of the mixed layer. At the RITS94 station the mixed layer depth varied from 90 to 120 m during the 4-day time series. At the RITS94 station the CO concentrations also decreased with depth through the mixed layer, but unlike the RITS93 station, there was a very strong gradient just below the bottom of the mixed layer. Because of the variability in the depth of the mixed layer (Figure 3b), sometimes the 100-m sample bottle was in the mixed layer and sometimes it was in the upper thermocline. This caused a large variability in the measured CO concentration at 100 m; when the 100-m sample bottle was in the mixed layer, CO concentrations were over 2 nM; when the 100-m sample bottle was below the bottom of the mixed layer, its CO concentrations were less than 1 nM.

The diurnal variation in CO column burden, driven by the daily photoproduction, is most apparent in the upper mixed layer and is shown in contour plots of CO concentrations to 75 m in Figures 4 and 5. Concurrent time series of total insolation and daily integrated insolation are also plotted in each of these figures. (Unfortunately, time series of UV light are not available for both stations.) The mean integrated daily sunlight was 19.5 MJ m^{-2} during RITS93 and 23.2 MJ m^{-2} during RITS94. Values were greater in the RITS94 time series due to the higher noon solar zenith angle (71° for RITS94, 62° for RITS93).

At both stations CO concentrations were at a maximum in the late afternoon at a depth of 5 or 10 m. These maximum concentrations were about a factor of 3 higher at the nutrient-rich RITS94 station. A diurnal pulse of warmer water is also seen in

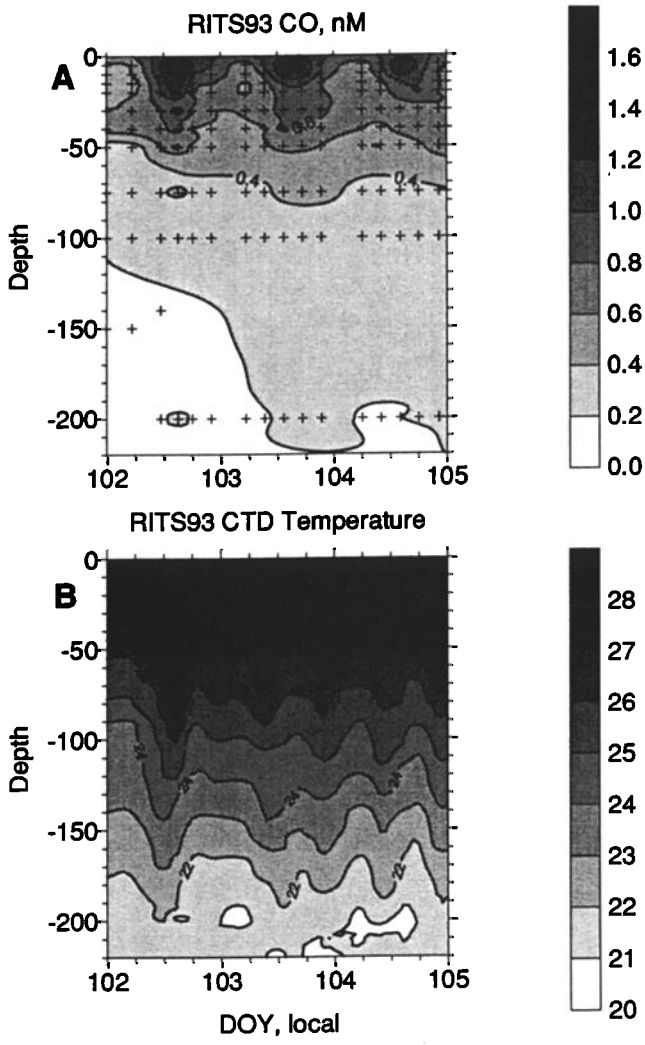

Figure 2. a) Contours in time and depth of CO concentrations at intervals of 0.2 nM for the RITS93 time series station. The position of the data points is also shown. The timescale is in decimal day of year (DOY) local time such that DOY 32.5 is local noon on February 1. b) Temperature contours in time and depth for the RITS93 time series station from the ship's conductivity-temperature-depth (CTD) system. The contour interval is 1°C. The bottom of the mixed layer is approximated by the 27-degree isotherm but is shown in better detail in Figure 4.

the temperature contours that has a close resemblance to the CO pulse. The temperature record from the RITS94 station, which followed a drifting buoy, was more consistent than that from the RITS93 station. The temperature varied over a range of 0.17°C at 35 m depth during RITS94. The temperature range at 35 m during RITS93 was 0.25°C , which included a 0.12°C cooling over a 4-hour period on the afternoon of day of year (DOY) 102, when a temperature front passed under the ship.

On the first and last days of the time series at the RITS93 station, the highest CO concentrations in the 5-m sample, 1.8 and 1.4 nM, respectively, occurred during the 1330 LT cast. On the second day of the time series the CO peaked during the 1730 LT cast with a concentration of 1.4 nm. On the three consecutive days minimum concentrations at the 5-m depth occurred during the 0530 LT cast and were 0.57, 0.62, and 0.72 nM, respectively. The temperature front on the afternoon of DOY 102 was coincident with a rapid decrease in CO that occurred in midafternoon, several hours earlier than on the other two days.

At the RITS94 station the daily maximum CO concentrations were recorded at 10 m depth (except at 5 m on DOY 343) at 1430 LT (except at 1830 LT on DOY 340). The daily maximum concentrations ranged from 3.8 to 4.4 nM. The daily minimum concentrations at 5 m depth all occurred during the 0630 LT cast and ranged from 2.9 to 3.3 nM.

Discussion

CO is photochemically produced and oxidized in the upper mixed layer but only oxidized in the lower mixed layer, due to the depletion of UV light there. Because the timescale of mixing

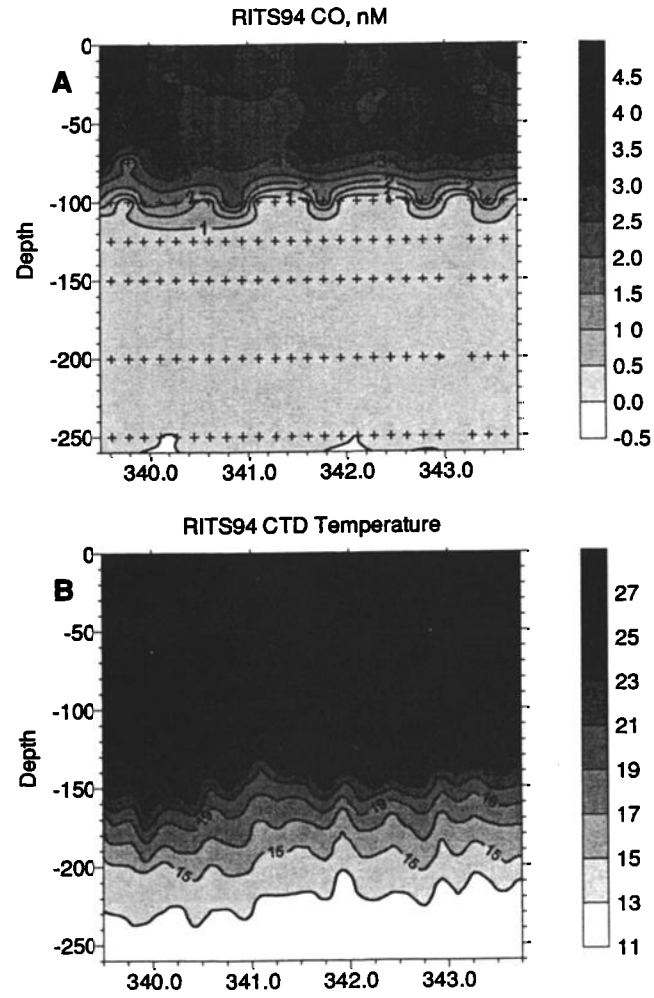

Figure 3. a) Contours in time and depth of CO concentrations at intervals of 0.5 nM for the RITS94 time series station. The position of the data points is also shown. The timescale is in decimal day of year (DOY) local time. b) Temperature contours in time and depth for the RITS94 time series station from the ship's CTD system. The contour interval is 2°C. The bottom of the mixed layer is approximated by the 27-degree isotherm.

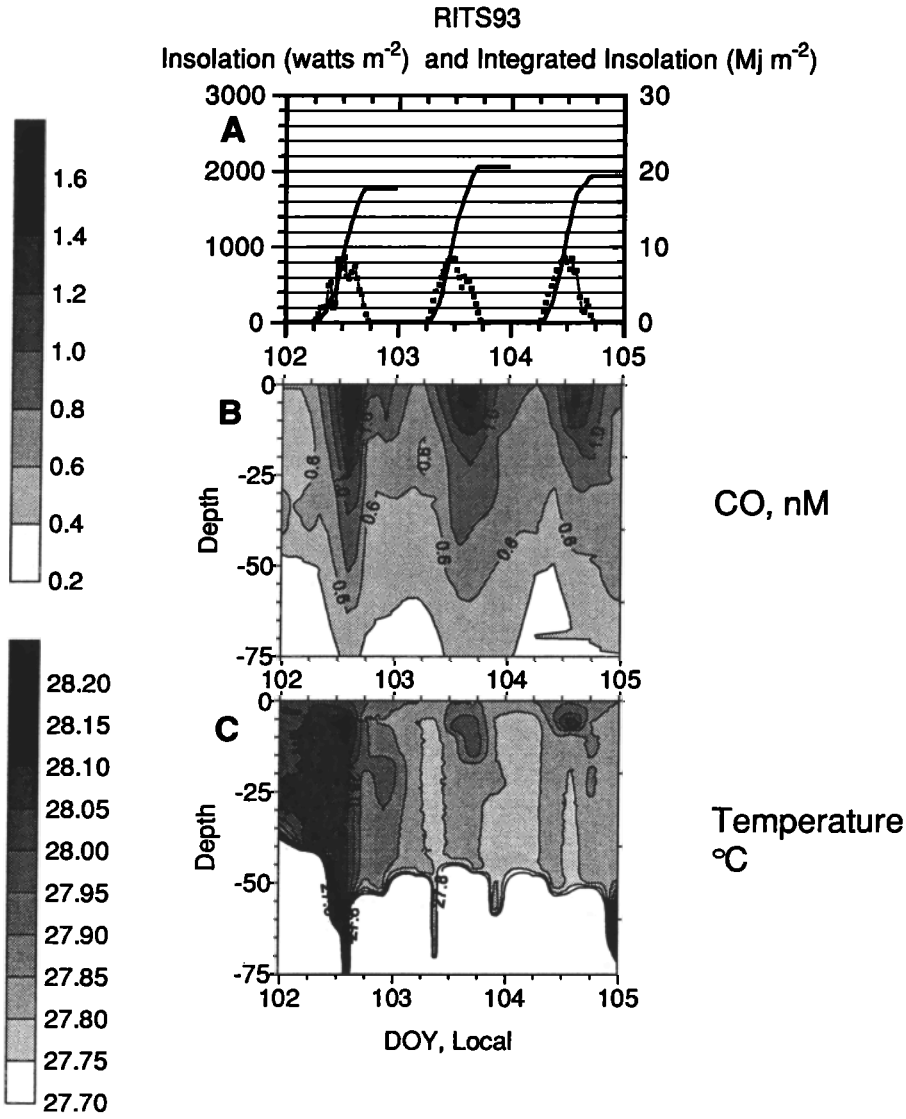

Figure 4. a) Time series of insolation in watts per square meter and daily integrated insolation in megajoules per square meter as functions of DOY local time measured by a shipboard Epply radiometer. b) CO data from Figure 2, contoured from 0 to 75 m depth to emphasize the diurnal pulse into the mixed layer. The contour interval is 0.2 nM. c) Temperature data from Figure 2, contoured from 0 to 75 m depth to emphasize the diurnal heating pulse into the mixed layer. The contour interval is 0.05°C. The bunching of the contour lines at the bottom of the figure defines the bottom of the mixed layer. Contours less than 27.7°C are not shown.

within the surface ocean mixed layer is a day or less [*McNeil and Farmer*, 1995], about an order of magnitude shorter than the lifetime of dissolved CO, the gradient of CO from the upper mixed layer to the lower mixed layer can be used to compare qualitatively the CO lifetimes at the two stations. At the RITS93 station the mean CO concentration at the bottom of the mixed layer (50 m) was 56% of the mean surface values. In contrast, at the RITS94 station, the mean CO concentration at the bottom of the deeper mixed layer (75 m) was 78% of the mean surface value. This suggests that the lifetime of CO at the RITS93 station was much shorter than at the RITS94 station.

The time series of the CO vertical distribution in the mixed layer can be used to quantify the CO production and loss rates if the various processes can be separated from each other. During the night the photochemical production goes to zero. Thus the nighttime decrease in the CO concentration results from only two mechanisms, sea-to-air exchange and oxidation. The sea-to-air exchange of CO can be calculated from parameterizations using partial pressure differences of CO in seawater and the atmosphere, and wind speed [*Bates et al.*, 1995]. The CO oxidation rate then can be calculated as the residual, and represents the in situ loss rate. From these measurements we have no way of determining the oxidation mechanism. However, previous investigations [*Conrad and Seiler*, 1980, 1982; *Jones*, 1991] strongly suggest that the in situ loss of CO in sea water is mediated entirely by microbial oxidation. Therefore we assume

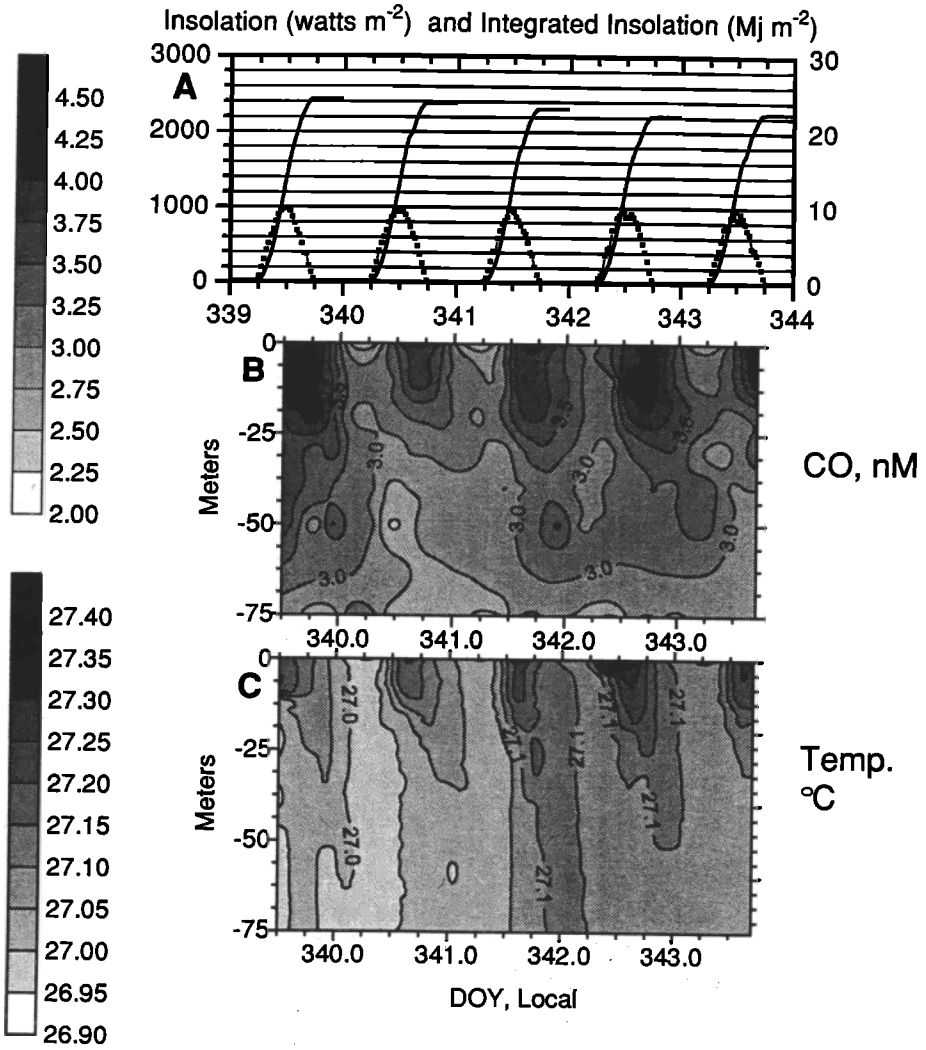

Figure 5. a) Time series of insolation in watts per square meter and daily integrated insolation in megajoules per square meter as functions of DOY local time measured by a shipboard Epply radiometer. b) CO data from Figure 3, contoured from 0 to 75 m depth to emphasize the diurnal pulse into the mixed layer. The contoured interval is 0.25 nM. c) Temperature data from Figure 3, contoured from 0 to 75 m depth to emphasize the diurnal heating pulse into the mixed layer. The contour interval is 0.05°C. Because the bottom of the mixed layer was near 100 m, there is no bunching of the contour lines as in Figure 4.

that our "oxidation" is microbial oxidation, and that the oxidation rate cannot be predicted from simple physical and chemical parameters such as temperature, pH, and oxygen concentration. We also assume that the bio-oxidation is linear, in that the loss rate is equal to the product of a loss rate constant and the CO concentration. This is a reasonable assumption if the primary loss process is microbial bio-oxidation via an enzyme-catalyzed reaction and if this enzyme is not saturated. We further make the assumption that the bio-oxidation rate was constant at each site over the time period of the measurements, but since the value of this oxidation rate constant depends on the microbial environment of the surface seawater, it can be different at the two sites. This oxidation rate constant is numerically equal to the reciprocal of the lifetime with respect to oxidation.

A final assumption that must be made in determining the production and loss rates from these two time series is one of horizontal uniformity. That is, CO concentration, production, and loss must be horizontally similar on a scale of tens of kilometers, so that horizontal mass fluxes and/or movement of the ship with respect to the oceanic mixed layer do not add extra terms to the mass continuity equation ((1) below). Ship motion relative to the water mass was much less at the RITS94 station, in that the ship followed a drifting drogue and remained with the same water mass during the time series station. Although the RITS93 station did not advect with the water mass, as shown below, the oxidation rate constant was much greater and the need for horizontal uniformity was not as severe.

One factor complicating the determination of the loss rate by observations of the CO depth-time series is that vertical mixing can affect the concentration change at any particular depth. However, as the column burden of CO in the mixed layer is not affected by vertical mixing, nocturnal decreases in the column

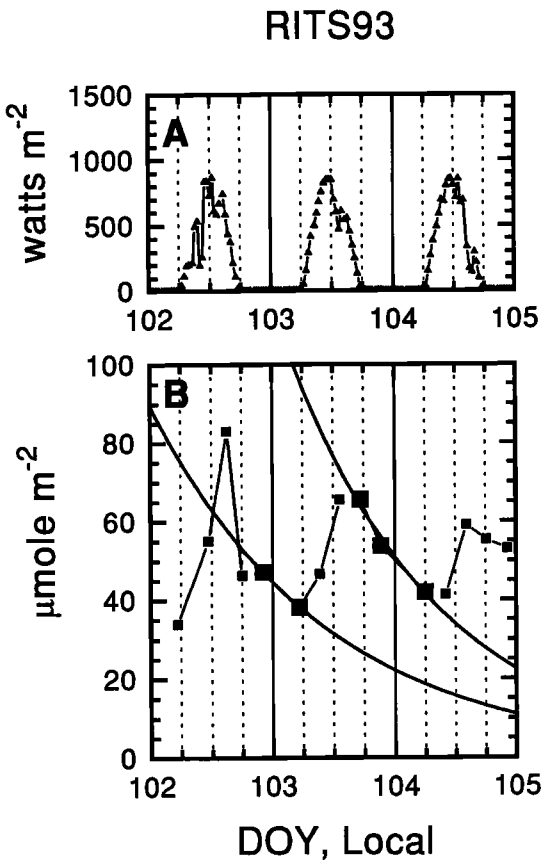

Figure 6. a) The insolation time series from Figure 4. b) Time series of the column burden of CO between 0 and 75 m in units of micromoles per square meter, integrated from the 10-point profiles by a method described in the text. The two heavy lines are exponential fits to the nighttime points. The points used for the fits are indicated by larger squares.

burden can be used to determine loss rates. The column burden of CO (0–75 m) was integrated for each concentration profile by drawing a line between each depth point and summing the areas of each resulting trapezoid (it was assumed that the concentration between 5 and 0 m was equal to the concentration at 5 m). The 75-m bottom for the column burden was chosen to avoid the large variability in CO concentrations at 100 m in the RITS94 record, which was due to the changes in the mixed layer depth. The resulting calculations, however, underestimate the RITS94 column burdens by approximately 20%.

The time series of the RITS93 CO column burden (Figure 6) shows afternoon maximum values of 83, 66, and 59 μmole m^{-2} d^{-1}, with daily increases from minimum to maximum of 59, 27, and 18 μmole m^{-2}, respectively. The column burden at the RITS94 stations (Figure 7) was much greater, with afternoon maximums of 270, 230, 260, and 260 μmole m^{-2}. However, the daily increases from minimum to maximum were similar to those at the RITS93 station: 19, 48, 37, and 15 μmole m^{-2}, respectively.

To determine the dissolved CO loss rates, loss times, and production rates, we employ three methods. The first method assumes that the production of CO is negligible during the night and that the loss is a first-order process. The first-order loss time then can be calculated by fitting the nocturnal sections of the CO column burden time series to an exponential function. The decay time calculated using this exponential fit method is the total loss time, which includes contributions from oxidation and sea-to-air flux.

For RITS93, the three data points from DOY 103.7 to 104.3 (1730 LT to 0530 LT, Figure 6) yield an exponential decay time or lifetime of 1.4 days. For the nocturnal decrease on DOY 103 the situation is complicated by the passage of the front that perturbed the CO concentrations between DOY 102.6 and DOY 102.75. Therefore we have used only the points from the casts at DOY 102.9 and 103.2 to derive an exponential decay time of 1.2 days. We did not calculate a decay time from casts 27 and 28 (DOY 105.2 to 105.4) because the ship left the station after cast 28 at 1000 LT, allowing only 4 hours to establish a decay time. Similar fits were made for the nocturnal decrease of the column burden at the RITS94 station. For the nights of DOY 340, 341, and 342 (Figure 7), the first-order decay times were 4.9, 3.4, and 6.8 days, respectively, considerably longer than at the RITS93 station. Table 1 lists the lifetimes of dissolved CO calculated by the exponential fit method for each day at each station, along with the estimated limits of uncertainty from propagation of the ±4.7% sampling error in the least square exponential fit.

The second method we use to calculate CO production and loss rates examines the day-to-night difference in the rate of change of the column burden. This method uses the individual

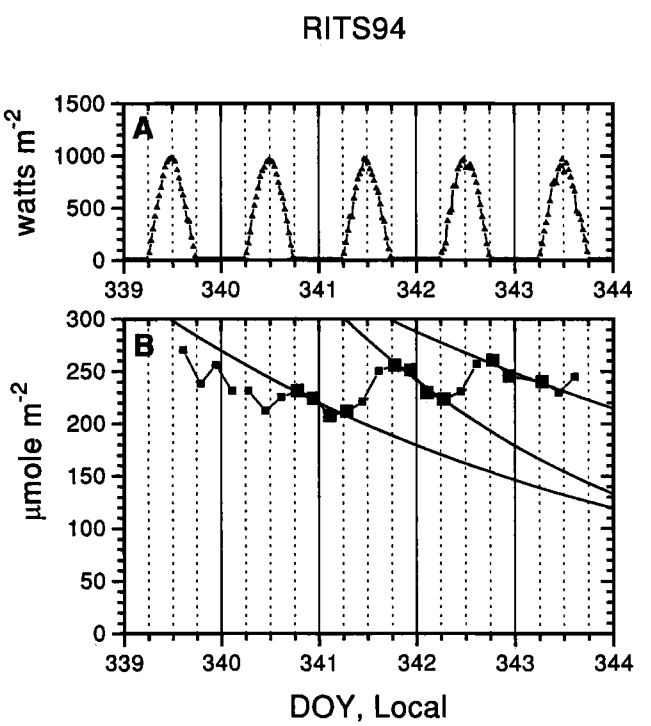

Figure 7. a) The insolation time series from Figure 5. b) Time series of the column burden of CO between 0 and 75 m in units of micromoles per square meter, integrated from the 12-point profiles by a method described in the text. The three heavy lines are exponential fits to the nighttime points. The points used for the fits are indicated by larger squares.

Table 1. CO Loss Rate Constants Calculated By Method 1, the Exponential Fit Method

Night	Loss Rate Constant, days^{-1}	Estimated Error, ±days^{-1}	Loss Time, days
102	0.699	0.216	1.4
103	0.817	0.124	1.2
RITS93 mean	0.758		1.3
340	0.204	0.122	4.9
341	0.298	0.124	3.4
342	0.146	0.128	6.8
RITS94 mean	0.216		5.0

This method predicts the total loss time, with contributions from oxidation and the sea-to-air flux. The data from Figures 6 and 7 were replotted with a logarithmic B axis and for each night a straight line was least squares fitted, the slope of each fitted line being the loss rate constant for that night. The estimated errors in the loss rate constants were derived from a propagation of the estimated sampling error (±4.7%) in the least squares fit. The loss time is the reciprocal of the loss rate constant.

terms in the continuity equation for the column burden of CO in the mixed layer:

$$\frac{dB}{dt} = P - L \tag{1}$$

where B is the column burden of CO, t is time, P is the column production rate, and L is the column loss rate. If the column loss rate is the sum of F, the sea-to-air flux, and λ, the oxidation rate, then (1) can be rewritten as

$$\frac{dB}{dt} = P - (F + \lambda). \tag{2}$$

The derivative dB/dt can be calculated numerically from the measured time series of B, F can be estimated from wind speed and CO surface concentration using a sea-to-air flux parameterization, and P can be assumed to go to zero at night, so the nighttime oxidation rate can be estimated as

$$\lambda = -\left(F + \frac{dB}{dt}\right). \tag{3}$$

If the daytime oxidation is assumed to equal the nighttime rate, then the daytime CO column production rate P can be estimated from

$$P = (F + \lambda) + \frac{dB}{dt} \tag{4}$$

using the nighttime value of λ from (3).

The results of this approach are shown in Figure 8 for the RITS93 station and Figure 9 for the RITS94 station. Figures 8a and 9a show the column burden interpolated onto even 30-min intervals. The dotted lines in Figures 8b and 9b show the numerically calculated time derivative of the column burden at each 30-min point in units of μmole m^{-2} d^{-1}. The sea-to-air flux, F, is shown in Figures 8c and 9c. F at each station was calculated from 30-min averages of the measured local wind speed, the *Wanninkhof* [1992] wind speed–transfer velocity algorithm with a Schmidt number for CO in seawater of 580 [*Bates et al.*, 1995], oceanic CO concentrations from the 5 m depth interpolated onto these time intervals, the mean measured atmospheric CO mixing ratios of 45 ppb at RITS93 and 66 ppb at RITS94, and the CO solubility relationship of *Wisenburg and Guinasso* [1979]. F has been added to the numerically calculated time derivative of B to give the solid line in Figures 8b and 9b. To reduce the short-term noise in the lines in Figures 8b and 9b, 12-hour averages were made to separate the daytime and nighttime fluxes (Figures 8d and 9d). The estimation of error in the calculation of the mean rates is not as straightforward as in the exponential fit method, where an accepted statistical algorithm can be used to estimate the propagation of measurement error. However, the errors in the calculated loss and production rates are likely comparable to those estimated with the first method. The errors in the calculation of air-sea fluxes also present difficulties, but following *Bates et al.* [1995] we estimate an uncertainty of a factor of 2.

The mean values for the nighttime loss rates, nighttime sea-to-air fluxes, nighttime oxidation rates, loss times, and daytime production rates calculated using this method are given in Table 2. For the RITS94 station the first 24-hour period did not give a clear diurnal cycle, so it has been excluded from the 12-hour mean rate plots and the results in Table 2. Using the final 3 days of RITS94, there is good agreement between the total loss time predicted by the exponential fit method (method 1) and by the derivative method (method 2), 5.0 and 5.3 days, respectively.

The agreement is not as good for the RITS93 station. Using the data from the night of DOY 103, both methods give nearly equivalent results. For DOY 102, however, both methods had problems resulting from the unusual pattern in the time series when a temperature front passed under the ship, resulting in a large decrease in the column burden in the late afternoon followed by an increase between 1800 and 2300 LT. This low loss during the nighttime produced a calculated lifetime of about 5 days for the night of DOY 102. For the exponential fit method this problem was eliminated by only using the two data points starting at 2230 LT, after the disturbance had passed, which yielded a loss time of 1.4 days. The passage of the front at the RITS93 station demonstrates the importance of making time

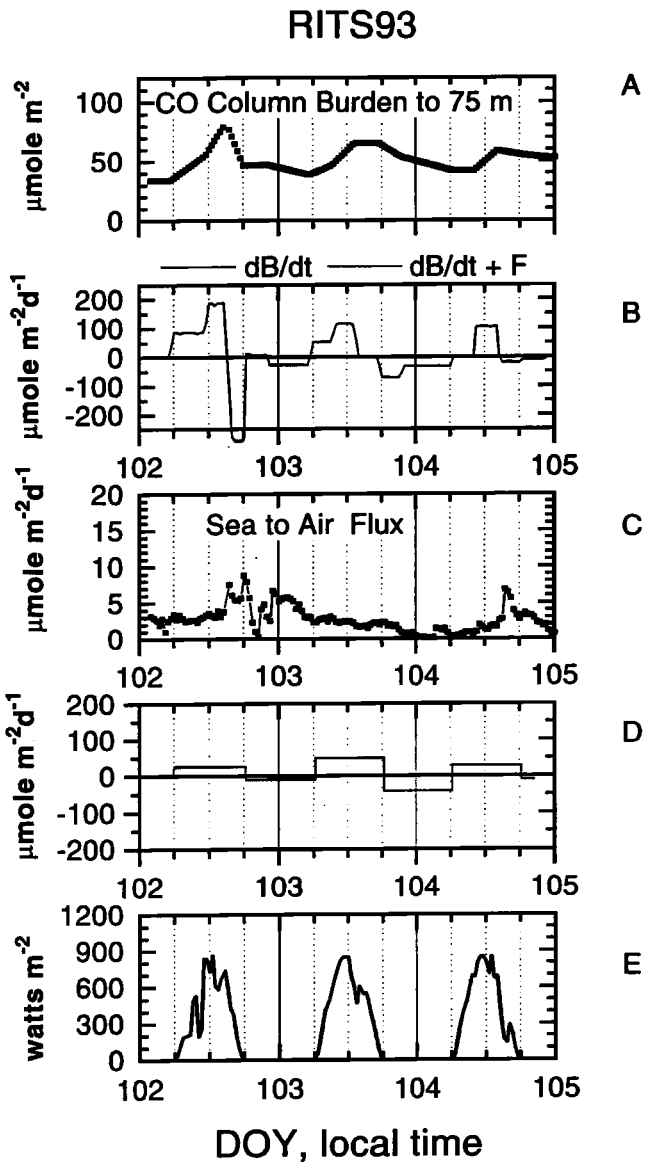

Figure 8. a) The column burden from RITS93 (Figure 6b) interpolated onto 30-min intervals. b) Dotted line is the numerically calculated time derivative of the column burden in units of micromoles per square meter per day. Solid line is the derivative added to the calculated sea-to-air flux of CO (see 8c). c) The sea-to-air flux of CO at 30-min intervals using the Wanninkhof exchange coefficient as described in the text. d) The values from 8b, averaged into 12-hour intervals to obtain the mean flux from each day and each night. e) The measured insolation.

series measurements over a period of at least 4 days and of following a single water mass.

The CO production rate derived from the second method at the RITS94 station was approximately 1.5 times that at the RITS93 station. The production of CO should scale with the amount of available UV light and with the amount of precursor material dissolved in the water column. Although continuous measurements of UV light were not available, the measured total insolation at the RITS94 station was 20% higher than at the RITS93 station, which is consistent with the difference in calculated production rates. DOC, the precursor of CO, was not measured at the two sites, but extrapolations of previous measurements along 140°W [*Peltzer and Hayward*, 1996] suggest that total organic carbon (which is comprised of >95% DOC) at the RITS93 station would be 25% higher than at the RITS94 station. This is contrary to the CO production rates calculated for the two sites. Although the available data cannot resolve the reason for the different production rates, this difference is small compared to the difference in the first-order oxidation time at the two sites.

The third method for calculating CO loss times uses a simple mathematical model of the diurnal cycle to estimate both the CO loss times as well as the phase of the diurnal cycle. If L from (1) is assumed to be linear and first order in B, then the loss term can be defined as

$$L = \frac{1}{\tau} B \tag{5}$$

where τ is the first-order loss time and is constant for each region. If the CO is in steady state such that its daily mean concentration is nearly constant from day to day, then τ is also the lifetime of CO in the mixed layer.

If the instantaneous production rate, P, is proportional to the available sunlight, then the time-dependent P should be represented by a clipped sine wave with a period of one cycle per day. Such a function would be difficult to solve mathematically, however. Therefore we assume that an offset sinusoid will

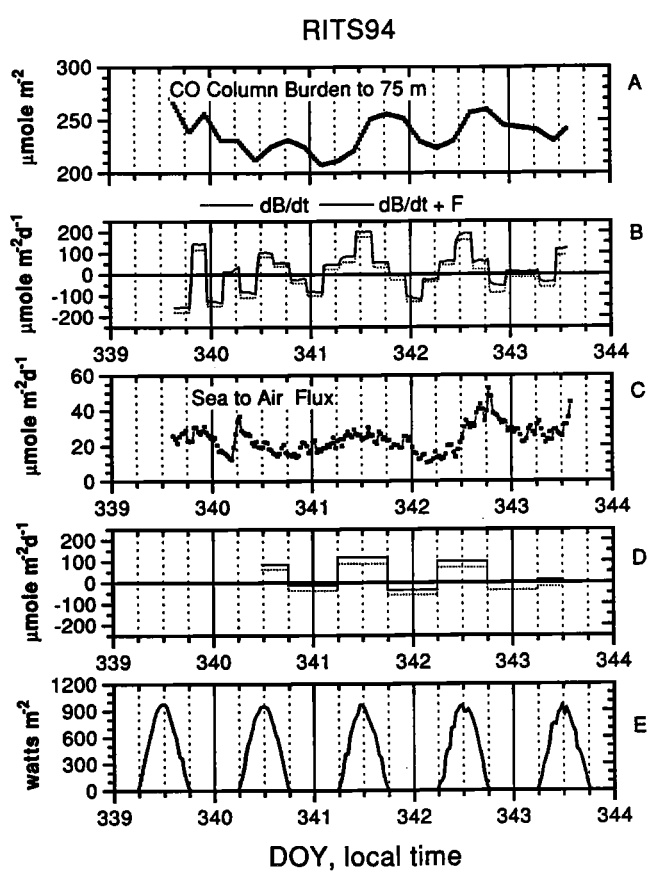

Figure 9. As in Figure 8 but for RITS94.

Table 2. CO Loss Rate Constants and Photo Production Calculated By Method 2: Using the Mean Rates From Nighttime (Loss Processes Only) and Daytime (Sum of Photoproduction and Loss Process)

Parameter	Units	RITS93	RITS94
Mean column burden	μmole m^{-2}	51.4	236.0
Nocturnal mean loss rates	μmole m^{-2} d^{-1}	25.9	44.8
Nocturnal mean air-sea flux	μmole m^{-2} d^{-1}	2.7	22.8
Mean oxidation loss rate	μmole m^{-2} d^{-1}	23.1	21.9
Oxidation rate constant	d^{-1}	0.455	0.093
Oxidation time	d	2.2	10.8
Sea-to-air flux time	d	19	10.3
Total loss time (or lifetime)	d	2.0	5.3
Mean rate of increase during daytime	μmole m^{-2} d^{-1}	32.7	59.1
Calculated photoproduction rate during daytime	μmole m^{-2} d^{-1}	55.8	83.3
Photoproduction per 24-hour day	μmole m^{-2}	27.9	41.7

The calculated daytime photoproduction rate is the mean photoproduction from 0600 to 1800 LT each day.

suffice:

$$P = A - A\cos(\omega t) \tag{6}$$

where t is the timescale in decimal days such that the fractional part of t is equal to zero at local midnight and equal to 0.5 at local noon, ω is the diurnal rate, 2π radians d^{-1}, and A is a constant for each region and season equal to one-half the maximum column production rate at local noon.

Substituting (5) and (6) into (1) yields

$$\frac{dB}{dt} = A - A\cos(\omega t) - \left(\frac{1}{\tau}\right)B \tag{7}$$

The solution of (7) is

$$B = ce^{\frac{-t}{\tau}} + A\tau - \frac{A}{\omega^2 + \frac{1}{\tau^2}}\left[\frac{1}{\tau}\cos(\omega t) + \omega\sin(\omega t)\right] \tag{8}$$

where c is a constant of integration and can be determined from initial conditions.

Equation (7) constitutes a simple model with an analytical solution (8). A more elaborate model with detailed physics can be found in work by *Doney et al.* [1995]. We do not claim that our simple model contains all of the relevant physics of mixing, light transmission, photoproduction, and bio-oxidation. Rather, we propose that the most important factors controlling the diurnal cycle of the column burden of CO are photochemical production and bio-oxidation and that, as shown below, this simple model with an analytical solution can qualitatively reproduce observed diurnal cycles and can deduce oxidation times that agree within a factor of 2 with other methods. This method also has the advantage of explaining the phase lag between the sunlight maximum and the concentration maximum.

If we are interested in the "steady-state" diurnal behavior, the first term in (8) can be neglected as it decays to zero with the time constant τ. The sin and cos terms can then be combined to arrive at a final steady state solution:

$$B = A\tau - \frac{A}{\sqrt{\omega^2 + \frac{1}{\tau^2}}}\cos(\omega t - \phi) \tag{9}$$

where ϕ is equal to $\tan^{-1}(\omega\tau)$ and is the phase angle in radians between the maximum in sunlight (noon) and the maximum in B; ϕ expressed in hours is $12\,\pi^{-1}\tan^{-1}(2\pi\tau)$. Figure 10a shows the predicted phase lag, in hours, as a function of loss time, τ. *Conrad et al.* [1982] reported that the surface water CO maximum concentration occurred 2–3 hours after local noon and attributed the phase lag to possible delayed production by photosensitized reactions involving oxygen radicals. This simple model demonstrates that a phase lag of 5–6 hours in peak column burden CO is expected for a CO lifetime of 0.6 days or longer, even with a peak production rate occurring at noon and no photosensitized delayed reaction. A possible reason that *Conrad et al.* [1982] saw a delay of 2–3 hours instead of 5–6 hours in surface water CO is that they were measuring surface water concentration and not column burden. CO in the surface water can diffuse downward and decrease surface CO concentration in the midafternoon, resulting in an earlier peak in surface concentration with no effect on column burden.

Although the predicted relationship between the CO lifetime and the measured phase lag in the CO column burden maximum can, in principle, be used to estimate the lifetime of CO in the mixed layer, in practice it can be seen that for all lifetimes greater than 0.6 days the phase lag will be between 5 and 6 hours. Although our two stations appeared to have a phase lag in the range of 4 to 6 hours, our time resolution in determination of B (4 hours) was too coarse to enable our measured phase lag to estimate the CO lifetime.

The diurnal cycle model also can be used to calculate a relationship between the relative diurnal amplitude of the CO column burden and the CO lifetime. This relationship can then be used to estimate the CO lifetime based on measurements of the diurnal amplitude. We define R to be the relative amplitude of the diurnal column burden variation, equal to the diurnal peak-to-peak amplitude of the column burden, ΔB, divided by

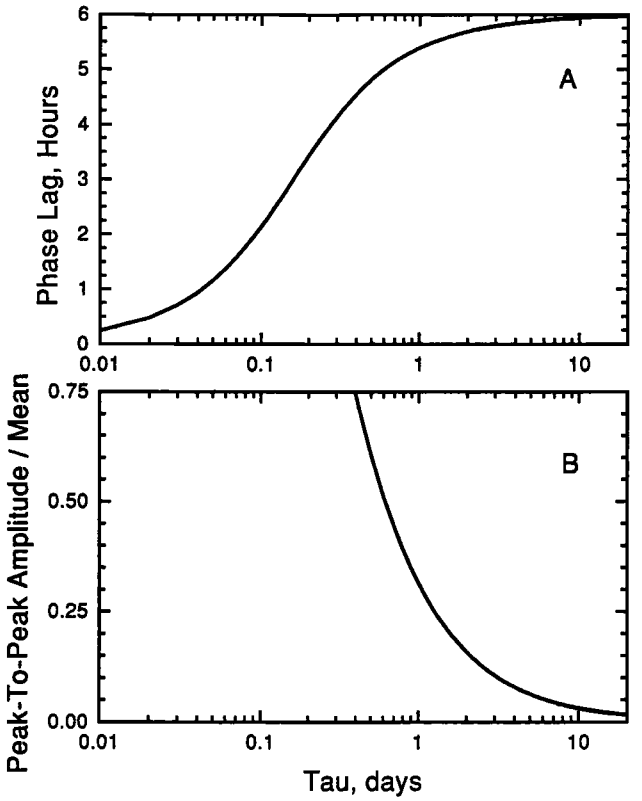

Figure 10. a) The phase lag in hours between the insolation maximum, local noon, and the maximum in the CO column burden as a function of CO loss time as predicted by the diurnal cycle model. b) The relative peak-to-peak amplitude of the diurnal cycle of the CO column burden as a function of the CO loss time as predicted by the diurnal cycle model.

the mean value of the column burden, $\bar{B}$. Because the first term on the right-hand side of (9) is the steady-state mean of the column burden, and the coefficient of the cos in the second term of (9) is one-half the peak-to-peak amplitude of the diurnal variation in the column burden, the simple model predicts R to equal

$$R = \frac{\Delta B}{\bar{B}} = \frac{2}{\tau\sqrt{\omega^2 + \frac{1}{\tau^2}}} \tag{10}$$

A plot of the relative amplitude as a function of lifetime (with ω equal to 2π radians d^{-1}) is shown in Figure 10b. Equation (10) can be rearranged to predict τ as a function of R:

$$\tau = \frac{\sqrt{\frac{4}{R^2} - 1}}{\omega} \tag{11}$$

For the RITS93 time series (Figure 6), the mean peak-to-peak amplitude of the diurnal oscillation is found to be 33 μmole m^{-2}, and $\bar{B}$ over that time is found to be 51 μmole m^{-2}, yielding a relative amplitude, R, of 0.63. For the RITS94 time series (Figure 7), $\Delta B = 32$ and $\bar{B} = 236$ (both in μmole m^{-2}), yielding an R of 0.14. Using equation (11), these R values predict lifetimes of 0.48 days for RITS93 and 2.35 days for RITS94 (Table 3). These loss times are about a factor of 2 less than those predicted by the other two methods although the ratio of the RITS93 to RITS94 CO loss times derived from the diurnal cycle model method is in the same range as the ratios predicted by the other two methods. The simplifying assumption that the instantaneous production rate can be represented by an offset sine wave may cause the model to underpredict the amplitude of the diurnal cycle for any given loss time, because the model is predicting some production occurring at all times during the night except midnight. Thus, for any measured peak-to-peak amplitude, the model underpredicts the loss time. Also, because the column burden was only sampled every 4 hours, the measured peak-to-peak amplitude may have been underestimated if the sample time did not correspond to the exact maximum and/or minimum in the column burden.

The loss times calculated by the exponential fit method and by the diurnal cycle model method are the total lifetimes including contributions from the sea-to-air flux and from in situ oxidation. The three lifetimes can be related as

$$\frac{1}{\tau_t} = \frac{1}{\tau_F} + \frac{1}{\tau_\lambda} \tag{12}$$

where τ_t is the total lifetime (or loss time), τ_F is the sea-to-air flux time (with respect to dissolved CO in the mixed layer), and τ_λ is the oxidation time. From data given in Table 2, τ_F is calculated to be 19 days at the RITS93 station and 10 days at the RITS94 station. The shorter sea-to-air flux times from RITS94 are due to a mean wind speed that was 1.7 times higher than at the RITS93 site. The predicted lifetimes with respect to oxidation using each method are shown in Table 4. Because the column burden at the RITS94 station was underestimated by approximately 20% due to CO in the mixed layer below 75 m, the predicted loss times in Table 4 have been increased by 20%. These loss times compare well to values reported by *Jones* [1991], who used radiochemical methods in the upper mixed layer of the Sargasso Sea to derive CO oxidation times of 1.1 to 3.9 days at two stations and 4 to 10 days at the third.

Table 3. CO Loss Time Predicted By Method 3, the Diurnal Cycle Model

Parameter	Units	RITS93	RITS94
Mean column burden	mole m^{-2}	51	236
Mean peak-to-peak amplitude	mole m^{-2}	33	32
Relative amplitude	(dimensionless)	0.63	0.14
Predicted loss time	d	0.48	2.4

Table 4. Predicted Total Lifetimes in Days Using Equation (12)

	RITS93	RITS94
τ_F	19	13
τ_t exponential fit	1.4	12
τ_t mean rate	2.2	14
τ_t diurnal cycle model	0.5	3.9

The lifetimes for RITS94 have been increased by 20% to account for underestimation of the column burden.

Of these three methods for estimating CO loss rates and lifetimes, the first is the most mathematically direct and allows the easiest determination of the propagation of the sampling error. The second method enables loss due to oxidation to be quantified and compared to the sea-to-air flux loss. The primary advantage of the third method is that it predicts a simple relationship between the diurnal amplitude and the lifetime of a photochemically produced compound. It also provides a simple procedure to determine the phase lag between the maximum in sunlight and the maximum in column burden.

As previously mentioned, 0.2 nM of CO was found at both stations from samples collected at 750 m depth where presumably no production was occurring. The residual concentration may represent a sample blank, or it may represent a residual CO concentration that arises from nonphotochemical sources. If it is a sample blank, then the 0–75 m column burdens at both stations have been overestimated by 15 μmole m^{-2}. This would represent a 6% overestimation of the column burden at the RITS94 station and a 29% overestimation at the RITS93 station. If this is the case, then estimated oxidation times need to be shortened by these factors.

Conclusions

At the RITS93 station, an oligotrophic site, surface CO concentrations varied from 0.58 to 1.8 nM and the CO column burden, integrated from 0 to 75 m depth, varied from 34 to 83 μmole m^{-2}. At the RITS94 station, located in the biologically productive equatorial region, surface CO concentrations varied from 2.9 to 4.2 nM and the CO column burden, integrated from 0 to 75 m depth, varied from 210 to 260 μmole m^{-2}.

By fitting the nocturnal decrease of CO to an exponential function, or by calculating the mean loss rate of CO during the night, the total lifetime of CO was 1.2 to 2 days at the RITS93 station and 3.4 to 6.8 days at the RITS94 station. The calculated sea-to-air flux of CO accounted for 10% of the CO loss at the RITS93 station and 50% of the loss at the RITS94 station. After accounting for the sea-to-air loss, the oxidation lifetime of CO was 1–2 days at the RITS93 station and 11 days at the RITS94 station.

A simple model of CO production and loss that relates the relative diurnal amplitude of the mixed layer CO column burden to the lifetime of CO yielded lifetimes somewhat shorter than those calculated by the nocturnal decrease methods. However, the ratio of the predicted lifetimes from each station using the simple model was similar to the ratio predicted from the nocturnal decrease method. The simple model also explains why measurements have shown that the peak in CO concentration occurs 3 to 6 hours after local noon.

We have shown time series of CO concentrations in the mixed layer of the tropical Pacific Ocean from two sites, one of which (RITS94) had CO surface concentration 3 times greater and a CO column burden 4.5 times greater than the other site. Although the CO photoproduction at the RITS94 site was 1.5 times greater than at the RITS93 site, this difference is insufficient to explain the concentration difference. The only factor that can explain this concentration difference is the in situ oxidation rate constant, which was 5 times larger at the RITS93 site. Although these measurements cannot distinguish between nonbiological and microbial oxidation, previous investigations suggest that this oxidation is meditated by bacteria [*Conrad and Seiler*, 1980] and may be related to the biomass of ammonia-oxidizing bacteria [*Jones et al.*, 1984]. Thus it appears that the local microbial oxidation rate constant, not the local production rate, may be the most important factor in determining the surface concentration of CO in much of the world's ocean.

Acknowledgments. Walter Helbling and Osmund Holm-Hansen provided the underwater UV irradiance profiles and the chlorophyll profiles at the RITS93 station. Ollie Zafiriou and Steven Andrews provided the irradiance profiles at the RITS94 station. We thank R. Feely and P. Quinn for comments on the manuscript. This work was carried out under the NOAA Radiatively Important Trace Species (RITS) Program and the Atmospheric Chemistry component of the NOAA Climate and Global Change Program. This is contribution 1521 from the NOAA Pacific Marine Environmental Laboratory and contribution 266 from the Joint Institute for the Study of the Atmosphere and Ocean.

References

Baker, K. S., and R. C. Smith, Spectral irradiance penetration in natural waters, in *The Role of Solar Ultraviolet Radiation in Marine Ecosystems*, edited by J. Calkins, pp. 233–246, Plenum, New York, 1982.

Bates, T. S., K. C. Kelly, and J. E. Johnson, Concentrations and fluxes of dissolved biogenic gases (DMS, CH_4 CO, and CO_2) in the equatorial Pacific during the SAGA 3 experiment, *J. Geophys. Res.*, *98*, 16,969–16,977, 1993.

Bates, T. S., K. C. Kelly, J. E. Johnson, and R. H. Gammon, Regional and seasonal variations in the flux of oceanic carbon monoxide to the atmosphere, *J. Geophys. Res.*, *100*, 23,093–23,101, 1995.

Conrad, R., and W. Seiler, Photooxidative production and microbial consumption of carbon monoxide in seawater, *FMES Microbiol. Lett.*, *9*, 61–64, 1980.

Conrad, R., and W. Seiler, Utilization of traces of carbon monoxide by aerobic oligotrophic microogranisms in ocean, lake, and soil, *Arch. Microbiol.*, *132*, 41–46, 1982.

Conrad, R., W. Seiler, G. Bunse, and H. Giehl, Carbon monoxide in seawater (Atlantic Ocean), *J. Geophys. Res.*, *87*, 8839–8852, 1982.

Doney, S. C., R. G. Najjar, and S. Stewart, Photochemistry, mixing and diurnal cycles in the upper ocean, *J. Mar. Res.*, *53*, 341–369, 1995.

Jones, R. D., Carbon monoxide and methane distribution and consumption in the photic zone of the Sargasso Sea, *Deep Sea Res.*, *38*, 625–635, 1991.

Jones, R. D., and J. A. Amador, Methane and carbon monoxide production, oxidation, and turnover times in the Caribbean Sea as influenced by the Orinoco River, *J. Geophys. Res.*, *98*, 2353–2359, 1993.

Jones, R. D., R. Y. Morita, and R. P. Griffiths, Method for estimating chemolithotrophic ammonium oxidation using carbon monoxide oxidation, *Mar. Ecol. Progr. Ser.*, *17*, 259–269, 1984.

McNeil, C. L., and D. M. Farmer, Observations of the influence of diurnal convection on upper ocean dissolved gas measurements, *J. Mar. Res.*, *53*, 151–169, 1995.

Mopper, M., X. Zhou, R. J. Kieber, D. J. Kieber, R. J. Sikorski, and R. D. Jones, Photochemical degradation of dissolved organic carbon and its impact on the oceanic carbon cycle, *Nature, 353*, 60–62, 1991.

Müller, J.-F., Geographical distribution and seasonal variation of surface emissions and deposition velocities of atmospheric trace gases, *J. Geophys. Res.*, *97*, 3787–3804, 1992.

Novelli, P. C., J. W. Elkins, and L. P. Steele, The development and evaluation of a gravimetric reference scale for measurements of atmospheric carbon monoxide, *J. Geophys. Res.*, *96*, 20,731–20,750, 1991.

Peltzer, E. T., and N. O. Hayward, Spatial and temporal variability of total organic carbon along 140°W in the equatorial Pacific Ocean in 1992, *Deep Sea Res. II*, in press, 1996.

Redden, G. D., Characteristics of photochemical production of carbon monoxide in seawater, M.Sc. thesis, Oregon State Univ., Corvallis, Oreg., 108 pp., 1983.

Seiler, W., and U. Schmidt, Dissolved nonconservative gases in seawater, in *The Sea*, vol. 5, pp. 219–243, edited by E. D. Goldberg, John Wiley, New York, 1974.

Smith, R. C., and K. S. Baker, Optical properties of the clearest natural waters (200–800 nm), *Appl. Opt.*, *20*, 177–184, 1981.

Swinnerton, J. W., and R. A. Lamontagne, Carbon monoxide in the South Pacific Ocean, *Tellus, 26*, 136–142, 1974.

Swinnerton, J. W., V. J. Linnenbom, and R. A. Lamontagne, The ocean: A natural source of carbon monoxide, *Science, 167*, 984–986, 1970.

Thompson, A. M., and R. J. Cicerone, Possible perturbations to atmospheric CO, CH_4, and OH, *J. Geophys. Res.*, *91*, 10,853–10,864, 1986.

Valentine, R. L., and R. G. Zepp, Formation of carbon monoxide from the photodegradation of terrestrial dissolved organic carbon in natural waters, *Environ. Sci. Technol.*, *27*, 409–412, 1993.

Wanninkhof, R., Relationship between wind speed and gas exchange over the ocean, *J. Geophys. Res.*, *97*, 7373–7382, 1992.

Wisenburg, D. A., and N. L. Guinasso, Jr., Equilibrium solubilities of methane, carbon monoxide and hydrogen in water and seawater, *J. Chem. Eng. Data, 24*, 356–360, 1979.

T. S. Bates and J. E. Johnson, Pacific Marine Environmental Laboratory, NOAA, Bldg. 3, 7600 Sand Point Way NE, Seattle, WA 98115. (e-mail: bates@pmel.noaa.gov; johnson@pmel.noaa.gov)

(Received June 15, 1995; revised January 26, 1996; accepted January 29, 1996.)